JOURNAL OF PROPULSION AND POWER
Vol. 17, No. 4, July–August 2001

Technical Notes

TECHNICAL NOTES are short manuscripts describing new developments or important results of a preliminary nature. These Notes cannot exceed 6 manuscript pages and 3 figures; a page of text may be substituted for a figure and vice versa. After informal review by the editors, they may be published within a few months of the date of receipt. Style requirements are the same as for regular contributions (see inside back cover).

Downstream Gas Effect on Nozzle Flow-Separation Location

John W. Murdock* and Richard P. Welle†
The Aerospace Corporation,
Los Angeles, California 90009-2957

I. Introduction

ON the first Titan IV flight (B-24) using solid rocket motor upgrades, the loads on the nozzle actuators caused by flow separation, just before launch, were higher than the predicted 3σ values and were not randomly oriented. It was hypothesized that the directional bias and increased magnitude were caused by having air on one side of the separated nozzle and exhaust from the solid-motor-powered gas turbines on the other. This hypothesis implicitly assumes that changing the gas external to the nozzle can change the flow separation location. This Note reports an experimental investigation to determine whether the gas external to a separated nozzle can affect flow separation location.

The idea that the downstream gas composition can affect the position of the flow separation point is new. Although there have been many studies of flow separation in nozzles, these works implicitly assume that the separation point is only a function of downstream pressure. The downstream gas is usually not mentioned, although it is most often air. Morrisette and Goldberg[1] give a compilation of such nozzle data.

II. Experimental Procedure

Flow separation is studied in a 15.7:1 area ratio conical nozzle.[2] This nozzle has a 12.80-mm-diam throat with five pressure taps in the divergent section. These taps, numbered P1–P5, are at area ratios 10.32, 8.80, 7.40, 6.11, and 3.91. The nozzle is fed by a reservoir containing either He or N_2. To control the external gas environment, the nozzle is contained in a coaxial 300-mm-diam pipe fed by a second reservoir. Tests are conducted with He nozzle gas exhausting into He, N_2, or SF_6 in the surrounding pipe and with N_2 exhausting into either He or N_2. Further details of the experimental apparatus are contained in Ref. 2. Flow separation at a given pressure tap in the supersonic nozzle section is studied by determining when the separation point passes the tap, first when the nozzle stagnation pressure rises during the transient nozzle start up and again when separation moves back upstream in the nozzle as the reservoir blows down.

III. Experimental Results

Data from a typical test with He nozzle gas exhausting into He background gas are shown in Figs. 1 and 2. (Pressure data are normalized with the atmospheric pressure P_a.) When nozzle flow first begins, the entire exit cone of the nozzle is separated and at 1 atm pressure. Figures 1 and 2 show the stagnation pressure P_c rising from 1 to nearly 100 atm in about one-third of a second, while the nozzle back pressure P_e remains constant. As the stagnation pressure rises, the pressure at a given exit-cone tap drops as a result of entrainment of the exit-cone gas into the primary flow. The pressure drop continues until the flow attaches, and then the pressure rises in proportion to the stagnation pressure. After the flow at all of the taps is attached, the stagnation pressure rises to its peak and begins to decay. The exit-cone taps now decay in proportion to the stagnation pressure, reaching a second relative minimum when the flow once again separates. After the flow separates during the blowdown, the pressure asymptotes to just below 1 atm. When separation has moved back upstream past the five taps, the test is terminated. We are, thus, able to obtain two sets of flow-separation data during each run, the rise data and the blowdown data. These separation pressures are defined by the two relative minimums at each exit-cone tap.

The data in Fig. 1 are used to investigate the separation during blowdown. These are 2000-Hz data that have been smoothed with a Gaussian filter; this process also reduces the data to a more manageable quantity. To study flow separation during the pressure rise,

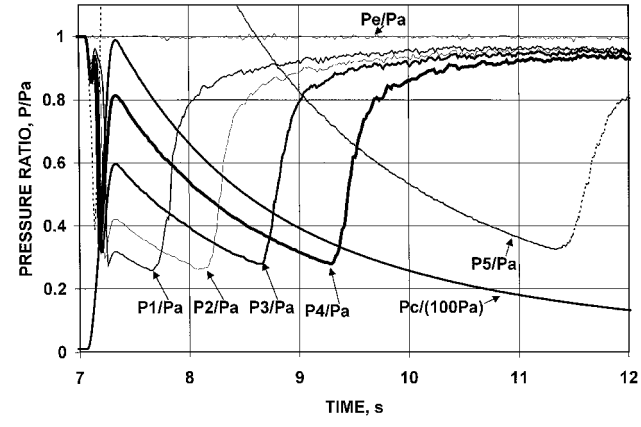

Fig. 1 Typical He–He pressures (filtered).

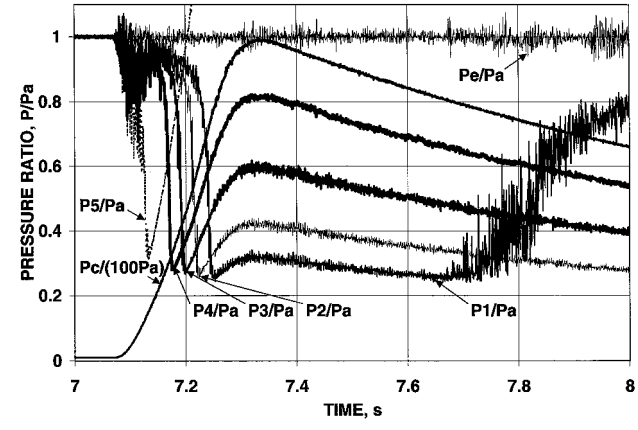

Fig. 2 Typical He–He pressures (unfiltered).

Presented as Paper 99-2644 at the AIAA/ASME/SAE/ASEE 35th Joint Propulsion Conference and Exhibit, Los Angeles, CA, 20–24 June 1999; received 5 July 1999; revision received 4 February 2001; accepted for publication 12 February 2001.

*Distinguished Engineer, Vehicle Performance Subdivision, P.O. Box 92957, M4-964. Associate Fellow AIAA.

†Manager, Fluid and Solid Mechanics Section, P.O. Box 92957, M5-753. Member AIAA.

we use the unfiltered data. Figure 2 shows an unfiltered version of Fig. 1. Comparing Figs. 1 and 2, we see that both the rise and blowdown data show the same trend; the separation (minimum) pressure decreases as the area ratio in the nozzle increases.

In this Note we are interested in differences in the mean or deterministic portion of the separation pressure caused by the presence of a downstream gas. (All separation data show a varying degree of randomness in the data.) A convenient and unambiguous way to characterize separation with a single parameter is to use the second relative minimum of the blowdown data curves (e.g., Fig. 1) and the first relative minimum of the rise data (Fig. 2). (In Fig. 1, the arrows identifying the data for taps 1–4 point to the blowdown separation point; in Fig. 2, arrows for taps 2–4 point to the rise separation point.) The minimum pressures probably do not correspond to actual boundary-layer separation; they more likely correspond to the locations in a flat plate boundary layer where the pressure first starts to rise before separation. However, in our data it is a well-defined pressure, and it is convenient to refer to it as the separation pressure for brevity.

Figure 3 shows the separation pressure normalized with the measured atmospheric pressure for the He blowdown data. These data are plotted as a function of nozzle-wall Mach number, which is computed from the measured pressures. The background gases were He, N_2, and SF_6. The filtering removes much of the randomness in the data; thus, most duplicate tests are well correlated.

One major exception is the He–SF_6 data at about Mach number 4.2. A large-scale separation-reattachment event occurred in two of the three runs at this Mach number and caused the large scatter. These events are one manifestation of the differences in flow character between the He–He and He–SF_6 data. These differences will be discussed further after considering steady separation.

Figure 3 shows that when He flows into a background gas of SF_6, the separation pressure is about 0.02 atm higher than is He into He. On the other hand, there is no measurable difference between the He–He data and the He–N_2 data. Shear-layer growth data discussed in Ref. 2 suggest a possible explanation for these results. Reduction of the He rise data shows that it is very similar to the blowdown data.[2]

Figure 4 shows the N_2 separation pressures with N_2 and He as background gases. The data show a higher separation pressure for N_2–He than for N_2–N_2. The pressure differences are smaller in Fig. 4 than in Fig. 3, but are still significant relative to the data scatter.

Figures 1–4 show the average separation pressures can change if the background gas is changed. There are also significant other changes. We now explore these briefly.

A comparison of the unfiltered data for He–He (such as that shown in Fig. 2) and similar data for He–SF_6 (Ref. 2) shows that the He–SF_6 data are noisier. These data, although only qualitative, indicate that the turbulence level is higher when He flows into SF_6 than when it flows into He.

Another way to contrast the different separation behavior is to overlay two sets of data with different background gases and the same nozzle gas. Such a comparison is shown in Fig. 5, in which He is the nozzle gas. The filtered SF_6 data have been time shifted

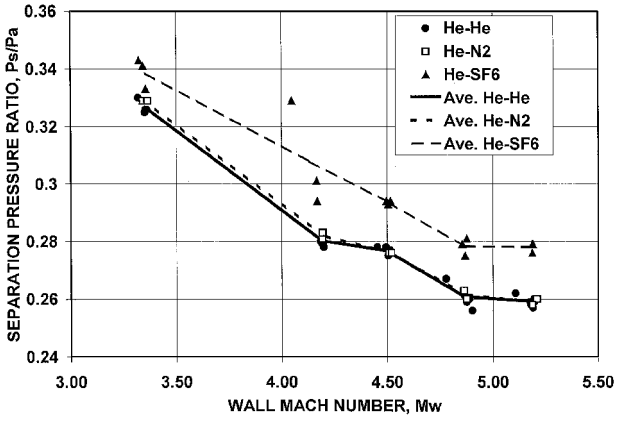

Fig. 3 Helium blowdown data.

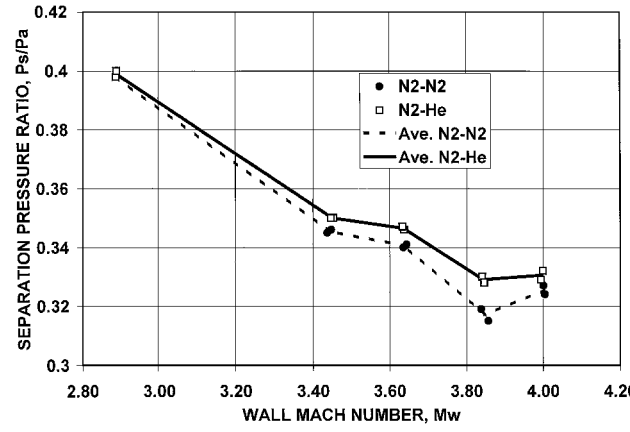

Fig. 4 Nitrogen blowdown Data.

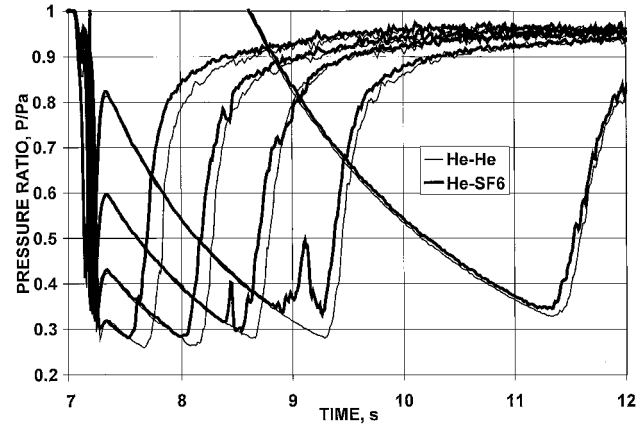

Fig. 5 Overlay of filtered helium separation data.

and overlain on the filtered data shown in Fig. 1. Particularly interesting are the large-scale, He–SF_6, separation–reattachment events seen at tap 3 at about 8.5 s and at the adjacent tap at about 9 s. Only one other event of this type was seen in the data, and it also was during an He–SF_6 run. Figure 5 shows that just recording the difference in the minimums of the various curves, as is done in Fig. 3, does not capture all of the differences in the data. The separation at different pressures results in a pressure difference until the plateau pressure is reached. Also, even the filtered He–SF_6 data are more unsteady or turbulent in the separated region, as the pressure rises from its minimum to the plateau, than are the He–He data.

These data suggest that earlier separation correlates with a higher turbulence level in the separated flow region. Reference 2 suggests that a larger shear-layer scale is correlated with earlier separation. These concepts are all related; a higher turbulence level produces a larger turbulent scale in the separated region, which in turn leads to a larger shear-layer scale.

IV. Concluding Remarks

To the authors' knowledge, no work before this Note has suggested that supersonic nozzle separation is affected by anything other than the downstream pressure. The data contained herein show that the gas composition downstream of the nozzle affects not only the boundary-layer separation pressure but also the turbulence level in the separated flow region. Thus, addressing the Titan engineering problem has resulted in the discovery of new phenomena influencing flow separation.

Acknowledgments

This work was supported in part by the Titan program office and in part by The Aerospace Corporation through the Mission Oriented Investigation and Experimentation Program. The authors

gratefully acknowledge the assistance of Andra Birkitt in preparing and operating the experiment.

References

[1]Morrisette, E. L., and Goldberg, T. J., "Turbulent-Flow Separation Criteria of Overexpanded Supersonic Nozzles," NASA Langley Research Center, NASA TP 1207, Hampton, VA, Aug. 1978.

[2]Murdock, J. W., and Welle, R. P., "Downstream Gas Effect on Nozzle Flow-Separation Location," AIAA Paper 99-2644, July 1999.

Adaptive Analysis of the Inviscid Supersonic Flow over a Backward-Facing Step

S. Y. Yang*
National Huwei Institute of Technology, Yunlin 632, Taiwan, Republic of China

Introduction

SEVERAL applications including scramjet, missile, rocket, and spacecraft may directly benefit from further understanding the supersonic flow over a backward-facing step. Research of flow separation and reattachment at supersonic speeds is commonly conducted in backward-facing step configurations. Such a flowfield can be described as a supersonic flow that turns beyond the step corner through an expansion fan and turns back to a direction approximately parallel to the inflow by an oblique reattachment shock wave. So far, numerous studies have been used to analyze supersonic backstep flows.[1–3] As mentioned by Venkatakrishnan,[4] unstructured grids provided flexibility for tessellating about complex geometry and for adapting to flow features, such as shocks. An underlying premise is that unstructured grid adaptation is far more automatable than are the tasks associated with multiblock structured grid generation. Recently, considerable effort has been made to develop solution-adaptive techniques[5–9] for solving the Euler/Navier–Stokes equations on unstructured meshes. By using the two-step Runge–Kutta Galerkin finite element method and a local remeshing technique,[5] a shock propagation within a channel was investigated. From the time-varying meshes directionally stretched elements were demonstrated. Webster et al.[6] developed an adaptive finite element methodology in which the finite quadtree mesh generator, interpolation-based error indicator, and edge-based mesh enrichment procedure were employed. On the quadrilateral-triangular mesh system Hwang and Fang[7] chose the magnitude of density gradient as an error indicator to perform the unsteady flow calculations, whereas Yang[8] took advantage of the absolute value of substantial derivative of Mach number as an error indicator to study oscillating cascade flows. The purpose of this work is to present a solution-adaptive solver to investigate the supersonic flow over a backward-facing step on mixed quadrilateral-triangular mesh. The Euler equations are solved in the Cartesian coordinate system. This solver includes the locally implicit scheme,[9] two-level refinement procedure,[7] and a modified error indicator.

Adaptive-Mesh Algorithm

The present adaptive algorithm includes the error indicator and two-level refinement technique. On quadrilateral-triangular meshes magnitude of density gradient[7] $|\nabla\rho|$ was employed as the error indicator to calculate the shock propagation in a channel, whereas the absolute value of substantial derivative of Mach number[8] $|DM/Dt|$ was chosen to capture the unsteady wave behavior and vortex-shedding phenomena. In the present calculations the steady solution is first achieved on the initial nonadaptive grid. According to the initial grid and steady solution, the adaptive mesh is accomplished using the error indicator and two-level refinement technique. Considering the supersonic flow over a backward-facing step, two mesh refinements are accomplished by choosing $|\nabla\rho|$ and $|\nabla M|$ as error indicators, respectively. It is found that neither of these two error indicators is capable of capturing the structure of the backstep corner vortex and expansion wave precisely. To capture the structure of the backstep corner vortex, the magnitude of gradient of vorticity magnitude $|\nabla\omega|$ ($\omega = |\nabla X \bar{V}|$, vorticity magnitude) is implemented as the error indicator to reperform the mesh refinement. According to the refined mesh, the structure of backstep corner vortex is captured clearly. However, it cannot capture the oblique shock and expansion wave behavior. Therefore, a modified error indicator is developed to capture the structure of backstep corner vortex, oblique shock wave, and expansion wave simultaneously. This modified error indicator EI can be written as follows:

$$EI = \frac{|\nabla P|}{|\nabla P|_{\max}} + \beta \frac{|\nabla\omega|}{|\nabla\omega|_{\max}} \tag{1}$$

where $|\nabla P|_{\max}$ and $|\nabla\omega|_{\max}$ are the maximum values of $|\nabla P|$ and $|\nabla\omega|$ among the computational cells. β represents the weighted coefficient and is chosen as 2.0. Because the order of magnitude of $|\nabla\omega|$ outnumbers that of $|\nabla P|$, it is essential to adjust both at the same order. Hence, $|\nabla P|$ and $|\nabla\omega|$ are divided by $|\nabla P|_{\max}$ and $|\nabla\omega|_{\max}$, respectively.

As for the two-level refinement technique, the value of EI of each unrefined cell is first calculated. The product of a specified constant C_1 and the average value of EI over the initial grid is selected as the first threshold value. If the value of EI of each unrefined cell is larger than the first threshold value C_1*$EIave$, the new node will be placed at the midpoint of each edge of quadrilateral/triangular cell or the center of quadrilateral cell.[7] After finishing the first-level refinement, the properties at all added new cells are interpolated from those at the initial grid. Continuing the second-level mesh refinement, the value of EI for each cell on the intermediate mesh and the corresponding second threshold value C_2*$EIave$ are computed. It is not necessary to perform any Euler iteration between level 1 and level 2 refinements. Normally, the value of constant C_2 is about two or three times bigger than that of constant C_1, and the value of constant C_1 ranges from 0.2 to 0.6. In the present calculation C_1 and C_2 are chosen as 0.4 and 1.0, respectively. Then the intermediate mesh is refined by reprocessing the first-level refinement technique. Because Webster et al.[6] mentioned that the mesh coarsening accounted for the majority of CPU cost during adaptation, the mesh coarsening procedure is not processed in this article.

Results and Discussion

The supersonic flow over a backward-facing step is investigated using the present solution algorithm. Geometric configuration and flowfield conditions are the same as those in the experiment.[2] Inlet Mach number, freestream temperature, freestream pressure, and velocity are set to 2.0, 167 K, 34.8 KPa, and 520 m/s, respectively. The averaged stagnation temperature and stagnation pressure measured in the experiment[2] were 310 K and 273 Kpa, respectively. The step height in the experiment was equal to 3.18 mm, whereas the width downstream of the backward-facing step was equal to 20.12 mm. The Mach 2 inlet flow expands through the centered Prandtl–Meyer expansion wave. A recirculation zone, which is essentially the backstep corner vortex, is formed behind the step and below the upper wall. Then the flow is turned back parallel to the upper wall and compressed through an oblique shock wave. The initial mesh shown in Fig. 1 incorporates the quadrilaterals and triangles, where the triangles are generated by the global remeshing algorithm.[5] This initial mesh may look like the multiblock grid with front quadrilaterals, intermediate triangles, and rear quadrilaterals,

Received 16 September 2000; revision received 24 February 2001; accepted for publication 23 March 2001.

*Associate Professor, Department of Aeronautical Engineering. Member AIAA.